MULTIPOINT MEASUREMENT OF WALL PRESSURE FLUCTUATIONS IN A SEPARATED AND REATTACHING FLOW OVER A BACKWARD-FACING STEP

Inwon Lee*
Department of Mechanical Engineering, KAIST
305-701 Taejon, Korea
s_liw@kaist.ac.kr

Hyung Jin Sung
Department of Mechanical Engineering, KAIST
305-701 Taejon, Korea
hjsung@kaist.ac.kr

ABSTRACT

Time-dependent characteristics of wall pressure fluctuations in separated and reattaching flows over a backward-facing step were investigated by means of continuous wavelet transform. Emphasis was placed on the combination of time-localized analyses of wavelet transform and multi-point measurements of pressure fluctuations. Synchronized wavelet maps revealed the evolutionary behavior of pressure fluctuations and gave further insight into the modulated nature of large-scale vortical structures. It was found that there exist two modes of shed vortices: one is the global oscillation and the other is the vortex convection. The two alternating modes are synchronized with the flapping frequency component of pressure fluctuations. Toward the investigation of the direct relationship between the flow field and the relevant spatial mode of the pressure field, a new kind of wavenumber filtering of pressure distribution, termed as a spatial box filtering (SBF), is introduced and examined. The conditional averaged velocity time history reveals that this SBF mode, tuned with the length scale of large-scale vortical structure, suggests its usefulness in capturing the large-scale coherent vortical structure.

INTRODUCTION

In a recent paper by the authors (Lee and Sung 2001, hereinafter referred to as LS), the spatial and spectral statistics of pressure fluctuations in separated and reattaching flows over a backward-facing step were reported. Multi-point measurements with an array of microphones in the streamwise and spanwise directions provided a comprehensive data file pertaining to the spatial characteristics of pressure fluctuations in the frequency domain. The coherence and wavenumber spectra exemplified the convective features which are closely associated with the large-scale vortical structures in the separated shear layer. The streamwise wavenumber spectra in LS, together with a preliminary calculation of the space-time cross-correlation, indicated the existence of a stationary mode and the scale variations of shed vortices. These suggested a modulated, intermittent spatio-temporal structure of shear layer under the flapping motion. A literature survey reveals that many studies have been made to find the mechanism of flapping motion in separated and reattching shear layers (Eaton and Johnston 1982, Kiya and Sasaki 1985, Le et al. 1997).

To scrutinize intermittent spatio-temporal behavior, a time-dependent analysis of vortical structure is highly desirable. In the present study, the unsteady behavior of pressure fluctuations in separated and reattaching flows over a backward-facing step is examined by means of continuous wavelet transform. Endowed with the wavelet's time-localized analysis capability, the present simultaneous, multipoint measurements of the pressure fluctuations furnish a novel technique to delineate the time-dependent nature of flow field. Emphasis is placed on the modulated spatio-temporal behavior of large-scale shed vortices in low frequencies. To further facilitate an in-depth in-

*This paper was supported by a grant from the National Research Laboratory of the Ministry of Science and Technology, Korea.

vestigation of the flow mechanisms pertaining to the low-frequency flapping motion and the large-scale vortex shedding process, an experimental technique was performed by measuring a joint correlation between the velocity field and the pressure fluctuations. An adequate online pressure data processing method, termed here as the spatial box filtering, will be introduced and discussed.

EXPERIMENTAL APPARATUS

A subsonic open-circuit wind tunnel, which had been constructed in the earlier work of Chun and Sung (1996), was slightly modified for the present experiment. A detailed description about the wind tunnel can be found in LS. The step height H of the backward-facing step was 50mm and the aspect ratio $AR = 12.5$. In the present study, an Acousticel array microphone system (The Modal Shop Inc., Model TMS130A) was utilized for sensing the pressure fluctuations. This system consists of 32 electret condenser microphones, with a diameter of 10.54 mm and a height of 25.4 mm, connection cables and a 32-channel differential amplifier (Model 514A). The calibration procedure is described in detail in LS, and the calibration results indicated that the magnitude error and the phase delay were below $\pm$1dB and $\pm$3 degrees, respectively, in the frequency range from 5 Hz to 10 kHz. This 'flat' response, together with the wide dynamic range of 42-142 dB, guarantees high levels of measurement accuracy without any further compensation procedure of the Acousticel output.

In the present measurement setup shown in Fig. 1, the array which consisted of 29 Acousticel microphones was located along the centreline of the test section. The array was set up with nonuniform interval so that it spanned a streamwise extent of $9H$ from $x/H = 2.0$ to $x/H = 11.0$. The interval between each microphone was set at $0.25H$ for the reattaching region $5.0 \leq x/H \leq 10.0$, while it was $0.5H$ for other regions. As seen in Fig. 1, velocity time history was measured on an (x, y)-centreplane of the test section. The velocity measurement grid of 37×21 extended over $2.0 \leq x/H \leq 11.0$ and $0.01 \leq y/H \leq 1.6$. For the measurement of the velocity field and time-mean reattachment length x_R, the usual hot-wire technique was used together with a constant temperature anemometer (TSI-IFA300). For every velocity time history measurement, pressure time history from a total of 29 microphones were simultaneously acquired using

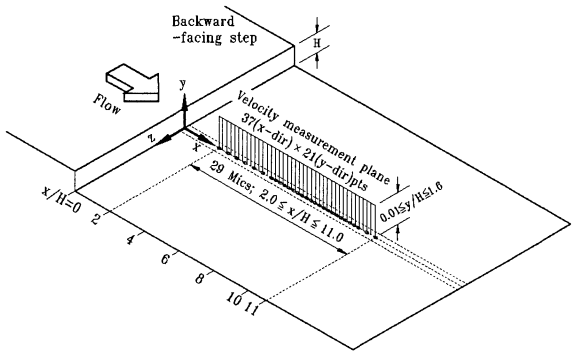

Figure 1: Schematic diagram of test section.

the 32-channel A/D converter DT2839 (Data Translation Inc.) with the effective sampling frequency of 488.28125Hz.

EXPERIMENTAL RESULTS

In the present experiment, the Reynolds number based on the step height $Re_H = 33{,}000$ is selected, which is the same as in the experiment of Chun and Sung (1996). When rescaled by using the momentum thickness, this corresponds to $Re_\theta = 1{,}300$. Among the various data representing the backward-facing step flow, the reattachment length x_R is frequently used as a representative quantity in a time-mean sense. The reattachment length is found to be $x_R = 7.4H$. Details regarding the mean and fluctuating velocity profiles and other quantities can be found in Chun and Sung (1996).

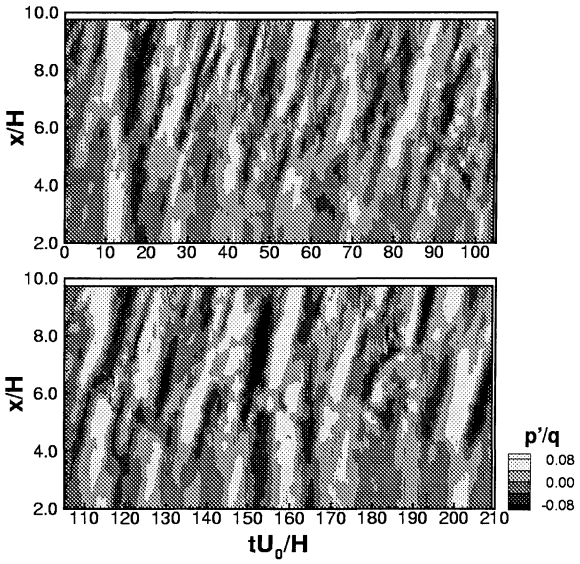

Figure 2: Space-time contour plots of pressure fluctuations.

To begin with, it would be advantageous to take a look at the global features of the space-time characteristics of wall pressure fluctuations. Figure 2 exhibit the space-time contour

plots of instantaneous wall pressure fluctuations, normalized by the freestream dynamic pressure $q = 1/2\rho U_0^2$, measured for $2.0 \leq x/H \leq 9.75$. Note that this figure consists of two 'time slides' with the upper one preceding the lower one. The downstream convective feature, denoted by an inclined contour pattern, is observed in both figures. There is no evidence of the upstream convection, which is consistent with the positive convection velocity estimation of $0.6U_0$ in LS. It is well known that the instantaneous negative peaks in wall pressure fluctuations are associated with the passage of large-scale vortices (Cherry et al. 1984, Kiya and Sasaki 1985). Also, the positive peaks are induced by the downward inrush of freestream between vortices. A closer inspection of Fig. 2 reveals that the pressure fluctuations are globally in phase and oscillate as a whole at some time instances, i.e., $tU_0/H \sim 10$ and 155. In addition, the pressure fluctuations are more intensive at this 'global oscillation' phase. Between the global oscillation phases, the convection of vortices seems to be prevailing. However, the strength and the spatial extent of each vortex are not uniform. Namely, relatively small scale behaviors are dominant at $tU_0/H \sim 40$.

To scrutinize the above modulated spatio-temporal behavior, a time-dependent analysis based on the wavelet transform is employed in this study. The wavelet transform has been extensively utilized as an analysis tool in turbulence studies. This popularity stems from the ability to elucidate both spectral and temporal information simultaneously. A comprehensive account of the mathematical and historical background of wavelet transform is given in Farge (1992). Endowed with the wavelet's time-localized analysis capability, the present simultaneous, multi-point measurements of the pressure fluctuations furnish a novel technique to delineate the time-dependent nature of flow field.

The wavelet transform $W(a,b)$ of a continuous real-valued time signal $x(t)$ is defined as the inner product between $x(t)$ and the analyzing wavelet $\psi_{a,b}(t) = (1/\sqrt{a})\,\psi((t-b)/a)$ (Farge 1992). Here, a is the timescale dilation parameter and b is the time translation parameter, respectively. Among the various wavelets proposed so far, consideration is given to a real-valued 'Mexican hat' wavelet, which is defined as, $\psi(t) = (1-t^2)\,e^{-t^2/2}$. Figure 3 shows the contour plots of wavelet transform, calculated at eight locations from the array with $X_0 = 2.0$

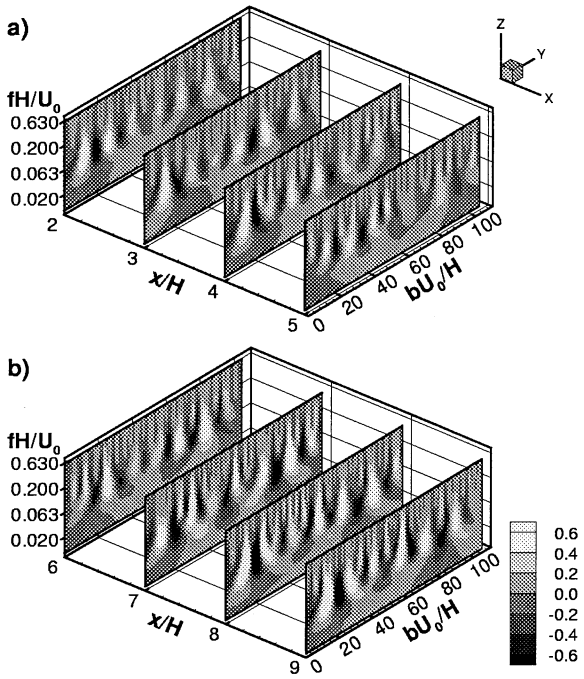

Figure 3: Contour plots of wavelet transform. a) $2.0 \leq x/H \leq 5.0$; b) $6.0 \leq x/H \leq 9.0$.

$(2.0 \leq x/H \leq 9.75)$ with the interval H. A nondimensional frequency fH/U_0 is employed on the z axis. As mentioned earlier, it is noteworthy that every plot of $W(a,b)$ has been synchronized because the pressure time histories from all points in the array are simultaneously acquired. Thus, the spatially-evolving characteristics of various frequency components can be displayed. The regular extrema along the frequency $fH/U_0 \sim 0.063$ correspond to the frequency of large-scale vortices, which was shown to be $fH/U_0 \sim 0.065$ in Fig. 3. It can be seen that this vortical component contains most energy of pressure fluctuations. This suggests that the shed vortices are largely responsible for the pressure fluctuations. The increase of rms pressure along the streamwise direction can be identified by simply comparing the maxima and minima of wavelet transform at various locations. A perusal of individual contour plots discloses that the large-scale vortical mode of pressure fluctuations undergoes energetic and quiescent phases. This tendency is evident in the forward part of the recirculation region (Fig. 3 a)).

In the reattaching region ($x/H = 8.0$ in Fig. 3 b)), the small-scale components are discernible near $bU_0/H \sim 40$. A closer inspection of both Fig. 2 and Fig. 3 b) indicates that the appearance of small scales is correlated with the initial stage of the vortex convection phase. At this stage, the separate

extrema with low and high frequencies demonstrate the breakdown of large-scale vortices. On the other hand, the contour plot exhibits simpler patterns in other stages. It seems that the frequency composition of eddies is influenced by the phase of flapping motion. Further downstream at $x/H = 9.0$, the small scale disturbances decay out and a new regular pattern is re-established. Eaton and Johnston (1981) reported the controversy between two models concerning the reattachment process; the downstream-moving small eddies in contrast to the eddies moving alternately upstream and downstream. The upstream convection has not been observed in the present wavelet transform analysis, which is consistent with the result in LS. Furthermore, the breakdown of eddies has not been observed at every large-scale vortical structure. Since the pressure fluctuations at a given point are in principle influenced by velocity fluctuations in the neighboring region of the flow, it seems to be inadequate to investigate the behavior of small scale eddies from the wavelet transform of pressure fluctuations. Nevertheless, it is obvious that the reattachment process gives rise to a multitude of events with different frequency compositions, rather than a unique predetermined one.

Since the wavelet transform is performed at each pressure time history, it may be possible to define the wavelet transform in a three-dimensional space (x, b, f). Accordingly, the isosurface of large magnitude of the wavelet transform, whose planform view is given in Fig. 4 a), represents a locus of high energy in the pressure fluctuations in space and time. The values of 0.6 and -0.6, approximately 40% of the maximum magnitude, have been chosen arbitrarily to define the isosurfaces. The alternating occurrences of the global oscillation phase and the vortex convection pahse are clearly seen in Fig. 4 a). Figure 4 b) is a cross-sectional contour plot of the wavelet transform at $fH/U_0 = 0.06458$, where the space-time variation of wavelet transform is most energetic. Note that the frequency corresponding to the most energetic scale coincides with the frequency of large-scale vortices ($fH/U_0 \sim 0.065$). At the beginning of the vortex convection phase near $bU_0/H \sim 50$, the inclined contours branch off from the vertical ones near $x/H = 4.0$. In addition, the end of the vortex convection phase is marked by a merging of the inclined contours back into the stationary vertical ones at $bU_0/H \sim 150$. These sequential phenomena can be described by the

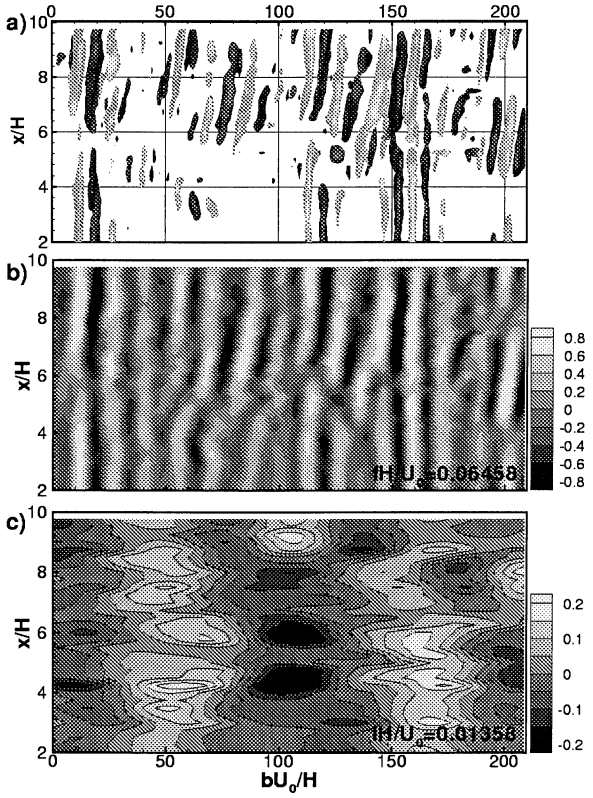

Figure 4: Planform views of wavelet transform. a) Isosurfaces; b) Contour plot at $fH/U_0 = 0.06458$; c) Contour plot at $fH/U_0 = 0.01358$.

following scenario of the large-scale vortices; firstly, a global intense oscillation appears with the contraction of separation bubble. As the bubble is enlarged, the separated shear layer receives positive momentum in the streamwise direction. After a quiescent period, a large-scale vortical structure emerges and is then accelerated to form orderly structure behind it. Secondly, these periodic vortices convect downstream. Finally, the vortices are decelerated and the next global oscillation redevelops.

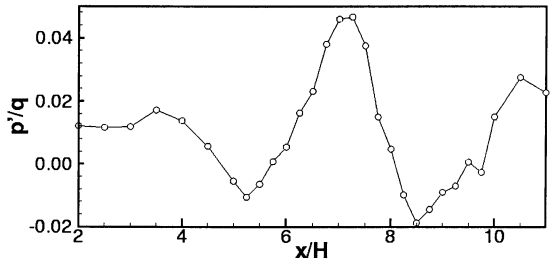

Figure 5: Streamwise distribution of the conditionally averaged pressure fluctuations.

The advantage of mulit-point pressure information over single point measurement as a conditioning signal is the immunity to irrelevant small scale mode contributions. In this respect, a relevant pressure component associated with the coherent structures in the flow

field could be found on the basis of the measured spatio-temporal distribution of pressure fluctuations. Toward this object, the appropriate length scale of the pressure field are to be found. This is implied in Fig. 5, where the streamwise distribution of conditionally averaged pressure fluctuations, normalized by the inflow dynamic pressure $(1/2\rho U_0^2)$, is presented. Time is synchronized with the the time when the transverse velocity fluctuations v' at $(x, y) = (7.5H, 1.0H)$ exceeds $-2.5v_{rms}$. It is seen that there exist a negative correlation between the pressure and v', and the pressure peak associated with the excursion of transverse velocity is of the order of $1.5p_{rms}$. The spatial distribution, the main peak surrounded by the negative upstream and downstream valleys, is attributable to the large-scale vortical structure. Kiya and Sasaki (1985) demontrated that the positive excursion of pressure fluctuation was shown to coincide with the inrush of the outer irrotational fluid with high total pressure towards the wall. The negative excursion of the transverse velocity imposed as the conditioning signal was indeed set toward to this inrush, the similarity between the two waveforms suggests that the conditional average of Fig. 5 results from the large-scale vortical structure. In this figure, and the spacing between the two valleys, which can be regarded as the spacing between large-scale vortices, is approximately $4H$. This spacing corresponds to $0.54x_R$, which is close to $0.6x_R$ reported by Kiya and Sasaki (1985).

From the above observation, it can be stated that the spatial mode of pressure fluctuations associated with the large-scale vortical structure attains a streamwise scale of $4H$. Of course, this is not to oversimplify the reattaching flow processes as a series of two-dimenisonal spanwise rollers. It is certain that the reattaching flow exhibits such inherent three-dimensionality as hairpin vortices and stremwise vortices in the shear layer, which was demonstrated by many researchers (Kiya and Sasaki 1985, Shih and Ho 1994, Le et al. 1997). However, it is no doubt that the most dominant source of pressure fluctuations is the spanwise large-scale vortical structure in the shear layer.

In order to extract a specific spatial component of the pressure field, a spatial box filtering (denoted as SBF hereinafter) is introduced in this study, whose schematic is given in Fig. 6. As depicted in Fig. 6, 16 equally-spaced microphones, with uniform spacing $\Delta x/H = 0.5$,

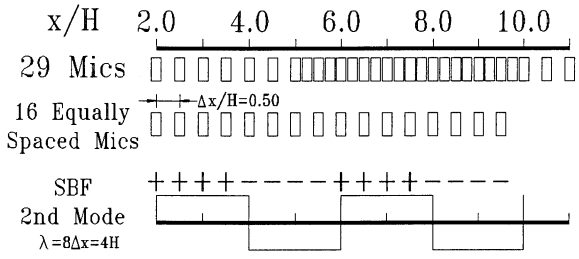

Figure 6: Schematic diagram of Spatial Box Filtering

out of whole 29-element array are utilized. The specific mode $\tilde{p}^{(i)}$ which corresponds to the spatial wavelength λ_i is obtained by a weighted sum of p_k, pressure at kth sensor, with a spatial filter function $w_k^{(i)}$ as follows:

$$\tilde{p}^{(i)} = \sum_{k=0}^{N-1} p_k w_k^{(i)}, \quad w_k^{(i)} = (-1)^{[k/2^{4-i}]}. \quad (1)$$

Here N is the number of sensor and $[\cdot]$ represents truncation to nearest smaller integer. Thus, the waveform of $w_k^{(i)}$ is a square wave whose wavelength λ_i is given as $2^{5-i}\Delta x = 2^{4-i}H$. The spatial box filtering (SBF) based on $w_k^{(i)}$ defined in the above equation is a wavenumber filtering tuned for a specific wavelength λ_i. As depicted in Fig. 6, the wavelength of $w_k^{(2)}$ is $4H$, the length scale of large-scale vortical structure. Therefore, the SBF 2nd mode of pressure $\tilde{p}^{(2)}$ represents the wavenumber components which is associated with the large-scale vortical structure.

The conditionally averaged velocity time histories $\langle u \rangle / U_0$ and $\langle v \rangle / U_0$ measured at $(x, y) = (7.5H, 1.0H)$ based on the SBF 2nd mode of pressure $\tilde{p}^{(2)}$ is shown in Fig. 7 a) and b), respectively. The conditional average based on the pressure fluctuations at $x/H = 7.5$ (denoted as p_R hereinafter) is also plotted as dashed line for comparison. The time is synchronized with the instants when the two conditioning signal, $\tilde{p}^{(2)}$ and p_R attains a peak over 2.5 times rms level of each signal. It is notable that the conditional averages based on $\tilde{p}^{(2)}$ show larger velocity excursions compared to those associated with local pressure peak. This implies that the randomness in the conditional average, which stems from the 'improper' conditioning peak in local pressure signal, i.e., pressure peaks uncorrelated with the coherent flow structures, has been reduced by means of utilizing an organized conditioning signal of SBF 2nd mode. The conditional averages in Fig. 7 show no appreciable information far from the zero time, say, $|tU_0/H| > 15$ due

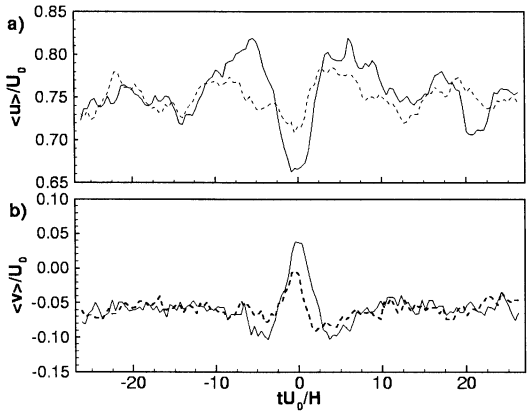

Figure 7: Comparison of the conditionally averaged velocity time history. ——, Conditional average based on $\tilde{p}^{(2)}$; - - -, based on the positive peak of p' at $x/H = 7.5$. a) $\langle u \rangle / U_0$; b) $\langle v \rangle / U_0$.

to the increasing uncertainties with respect to the increase in the time difference. However, the conditionally averaged velocity excursions based on both signal become nearly coincident, although not exactly. From this, the conditioning signal of $\tilde{p}^{(2)}$ can be regarded to be largely in phase with the coherent component near the time-mean reattachment point $x_R/H = 7.4$. In summary, it can be stated that $\tilde{p}^{(2)}$ is more closely associated with the pressure-generating coherent flow structure than the pressure a single location. Furthermore, this pressure mode is readily applicable to the a non-intrusive online investigation of the large-scale vortical structures.

CONCLUDING REMARKS

Unsteady characteristics of wall pressure fluctuations in the separated and reattaching flows over a backward-facing step and their relationship between relevant flow modes have been described by means of a variety of signal processing methods. In the present study, the wavelet analysis of pressure time histories from an array of microphones elucidated various evolutionary features of flow field. It was found that the periodic maxima and minima of the wavelet transform are mainly concentrated at the frequency of large-scale vortical structure. The shed vortices play a major role in generating the pressure fluctuations. There exist two modes of shed vortices; one is the global oscillation and the other is the vortex convection. These are synchronized with the flapping frequency component of pressure fluctuations p_F and a possible scenario of the vortical motion is then proposed. From the space-time information of the pressure fluctuations, an effective means to extract relevant spatial mode due to the large-scale vortical structure has been introduced and discussed. This is termed as spatial box filtering (SBF) and the emphasis is given to the SBF 2nd mode of pressure $\tilde{p}^{(2)}$ with the wavelength corresponding to the length scale of the large-scale vortical structure. The conditional average of velocity fluctuations based on $\tilde{p}^{(2)}$ reveals that this mode is better correlated with the pressure-generating eddies than the pressure at a single location.

REFERENCES

Cherry, N. J., Hillier, R. and Latour, M. E. M. P., 1984, "Unsteady measurements in a separated and reattaching flow", *J. Fluid Mech.*, Vol.144, pp.13-46

Chun, K. B. and Sung, H. J., 1996, "Control of turbulent separated flow over a backward-facing step", *Exp. Fluids*, Vol.21, pp.417-426.

Eaton, J. K. and Johnston, J. P., 1981, "A review of research on subsonic turbulent flow reattachment", *AIAA J.*, Vol.19, pp.1093-1100.

Eaton, J. K. and Johnston, J. P., 1982, "Low frequency unsteadiness of a reattaching turbulent shear layer", *Turbulent Shear Flows*, Vol.3, pp.162-170.

Farge, M., 1992, "Wavelet transforms and their application to turbulence", *Ann. Rev. Fluid Mech.*, Vol.24, pp.395-437.

Kiya, M. and Sasaki, K., 1985, "Structure of large-scale vortices and unsteady reverse flow in the reattaching zone of a turbulent separation bubble", *J. Fluid Mech.*, Vol.154, pp.463-491.

Le, H., Moin, P. and Kim, J., 1997, "Direct numerical simulation of turbulent flow over a backward-facing step", *J. Fluid Mech.*, Vol.330, pp.349-374.

Lee, I. and Sung, H. J., 2001, "Characteristics of wall pressure fluctuations in separated flows over a backward-facing step Part. I Time-mean statistics and cross-spectral analyses", *Exp. Fluids*, Vol.30, pp.262-272.

Shih, C. and Ho, C. M., 1994, "Three-dimensional recirculation flow in a backward facing step", *J. Fluids Eng.*, Vol.116, pp.228-232.